Continuous-time quantum walks with defects and disorder

J. A. Izaac,* J. B. Wang,† and Z. J. Li
School of Physics, The University of Western Australia, Crawley WA 6009, Australia
(Received 6 August 2013; published 29 October 2013)

With the advent of physical implementations of quantum walks, a general theoretical and efficient numerical framework is required for the study of their interactions with defects and disorder. In this paper, we derive analytic expressions for the eigenstates of a one-dimensional continuous-time quantum walk interacting with a single defect, before investigating the effects of multiple diagonal defects and disorder, with emphasis on its transmission and reflection properties. Complex resonance behavior is demonstrated, showing alternating bands of zero and perfect transmission for various defect parameters. Furthermore, we provide an efficient numerical method to characterize quantum walks in the presence of diagonal disorder, paving the way for selective control of quantum walks via the optimization of position-dependent defects. The numerical method can be readily extended to higher dimensions and multiple interacting walkers.

DOI: 10.1103/PhysRevA.88.042334 PACS number(s): 03.67.Lx, 05.40.Fb, 05.45.Mt

I. INTRODUCTION

Since the seminal paper by Aharonov *et al*. [1] establishing a quantum analogy of the classical walk, quantum walks have constituted an important tool in quantum information theory; for example, by motivating the creation of quantum algorithms that are faster and more efficient than their classical analogues [2–8] and by providing methods of universal quantum computation [9–11]—a highly sought-after goal of modern physics. This is a consequence of the markedly different behavior exhibited by quantum walks: by taking into account superposition, interference, and quantum correlations, the quantum walkers propagate quadratically faster than their classical counterpart and result in a probability distribution drastically different from the classically expected behavior [2]. As with classical random walks, there are two related but fundamentally different formulations of the quantum walk: the discrete-time quantum walk (DTQW) and the continuous-time quantum walk (CTQW). While these are related through well-defined limits in the classical case, their relation in the quantum realm is highly nontrivial, as shown by Strauch [12]. In this paper, we will focus on the continuous-time quantum walk, with emphasis on its scattering behavior in the presence of disorder and defects.

Quantum walks have proven incredibly versatile in terms of theoretical applications, with uses ranging from implementing quantum algorithms to modeling complex quantum systems. In order to benefit from these newfound ideas, physical implementations are essential; some recent approaches include the use of waveguides and photonics [13–16] and ion lattices [17–19]. With physical implementations of quantum walks comes the issue of disorder and decoherence affecting the sought after quantum behavior. In a precursor to modern quantum walking systems, the limiting case of a single diagonal defect in a one-dimensional molecular crystal was explored quantitatively by Koster and Slater [20] using tight-binding methods and difference equations, and later extended to take into account nearest-neighbor interactions (resulting in very effective exciton traps) [21]. Some earlier works by Dean [22] and Thouless [23] also looked at multiple defects in relation to the density and distribution of eigenstates. Such a tight-binding lattice model has found applications in a wide variety of fields. For example, Avgin and Huber [24] applied the one-dimensional, single impurity model to study defects in polyfluorenes.

More recently, the theoretical effects of random disorder in quantum walks have been considered by Yin *et al*. [25], Schreiber *et al*. [26], and Mülken and Blumen [27] (the latter also considering the effects of nonunitary "traps"). Disorder and decoherence, however, may provide additional tools in constructing quantum walks for particular applications—for instance, Keating *et al*. [28] considered the application of disorder-induced Anderson localization in quantum communication. In this work, the point-defect model of diagonal disorder, which is similar to that of Koster and Slater [20], will be used to derive expressions for the CTQW eigenstates for transmission through a single defect. This will then be extended to provide transmission amplitudes through multiple defects and, in particular, highlight resonant and bandlike structures. Furthermore, a general numerical method will be developed that efficiently calculates transmission information for an arbitrary distribution of diagonal defects, allowing a detailed study of defect-induced selective transmission of continuous-time quantum walkers.

This paper is structured as follows. In Sec. II, we introduce the mathematical formalism behind continuous-time quantum walks and, in particular, the diagonal point-defect model. Analytic expressions for the single-defect eigenstates are presented in Sec. III. Expressions for CTQW transmission through multiple, equally spaced defects are then derived in Sec. IV and used to verify the results of a general numerical method for arbitrary defect distributions, which is detailed in Sec. V. Finally, our conclusions are provided in Sec. VI.

II. CTQW DIAGONAL DEFECT MODEL

Continuous-time quantum walks were first introduced by Farhi and Gutmann [29] in 1998 as an extension of the classical theory of Markov processes. While research into continuous-time quantum walks has not been as extensive

*josh.izaac@uwa.edu.au
†wang@physics.uwa.edu.au

as the discrete-time case, some applications that have arisen include efficient spatial search algorithms that achieve a speedup of $\sqrt{N}$ over classical counterparts [4], exploring topological structure [30], and modeling coherent transport on complex networks [27] (such as mass and energy transport in complex molecular structures). Furthermore, recent experimental evidence for energy transfer through quantum coherence in photosynthetic and other biochemical systems [31–34] suggests that continuous-time quantum walks can be extended to model biological systems—potentially providing new insights into the natural world.

The continuous-time quantum walk can be regarded as a quantization of the corresponding classical continuous-time random walk, with the system now evolving as per the Schrödinger equation rather than the Markovian master equation. As a result, classical probabilities are replaced by quantum probability amplitudes. To illustrate, consider a continuous-time random walk on the discrete graph $G(V,E)$, composed of unordered vertices $j \in V$ and edges $e_i = (j,k) \in E$ connecting two vertices j and k. The transition rate matrix H is defined as

$$H_{jk} = \begin{cases} -\gamma_{jk} & \text{for } j \neq k \text{ if node } j \text{ is connected to node } k \\ 0 & \text{for } j \neq k \text{ if node } j \text{ is not connected to node } k \\ S_j & \text{for } j = k, \end{cases} \tag{1}$$

where γ_{jk} is the probability per unit time for making a transition from node j to node k and for H to be conservative,

$$S_j = \sum_{k=1, k\neq j}^{N} \gamma_{jk}. \tag{2}$$

Classically, the state of the random walker is fully described by the probability distribution vector $\mathbf{P}(t)$, with its time evolution governed by the master equation

$$\frac{d\mathbf{P}(t)}{dt} = H\mathbf{P}(t),$$

which has the formal solution $\mathbf{P}(t) = \exp(-Ht)\mathbf{P}(0)$.

Extending the above description to the quantum realm involves replacing the real-valued probability distribution vector $\mathbf{P}(t)$ with a complex-valued wave function $|\psi(t)\rangle$ and adding the complex notation i to the evolution exponent, i.e.,

$$|\psi(t)\rangle = \exp(-iHt)|\psi(0)\rangle. \tag{3}$$

The quantum transition matrix H, often referred to as the system Hamiltonian, is required to be Hermitian and thus the above time evolution is unitary—guaranteeing that the norm of $|\psi(t)\rangle$ is conserved under CTQWs. The complex-valued state vector $|\psi(t)\rangle = \sum_j a_j(t)|j\rangle$, where $a_j(t) = \langle j|\psi(t)\rangle \in \mathbb{C}$, represents the probability amplitude of the walker being found at node $|j\rangle$ at time t, with $|a_j(t)|^2 = |\langle j|\psi(t)\rangle|^2$ the resulting probability.

For CTQWs on an infinite line, if each node is assumed to be connected only to its neighboring nodes by a constant transition rate $\gamma = 1$, then the action of the corresponding Hamiltonian H_0 on the state vector $|\psi(t)\rangle$ leads to the inner product relationship

$$\langle j|H_0|\psi\rangle = 2\langle j|\psi\rangle - \langle j+1|\psi\rangle - \langle j-1|\psi\rangle. \tag{4}$$

Symmetries that are present in continuous-space quantum systems, for instance invariance under spatial translation for free particles, can also be formulated for discrete-space systems. This symmetry allows us to define the momentum eigenstate $|k\rangle$: a complete orthonormal basis of the Hamiltonian, satisfying the eigenvalue equation $H_0|k\rangle = 2(1-\cos k)|k\rangle$ for $-\pi \leqslant k < \pi$. Analogous in function to the momentum eigenstates encountered in continuous-space quantum mechanics, these are an important tool in studying scattering properties in discrete space and, as such, have been described in detail by Childs *et al.* [3], Farhi *et al.* [10], Mülken and Blumen [27], Childs and Gosset [11], Mülken *et al.* [35], and Childs *et al.* [36] (albeit with slight variations in definition). For example, consider a continuous-time quantum walk on an infinite line, scattering off a defect placed at node $|d\rangle$. To account for these defects, the Hamiltonian matrix is modified in the following way:

$$H = H_0 + \Gamma, \quad \Gamma = \sum_m \Gamma_m |m\rangle\langle m|, \tag{5}$$

where we have introduced a real diagonal matrix Γ, with $m \in \mathbb{Z}, m \in \{d\}$ representing the set of vertices associated with a defect of strength Γ_m. The probability of the walker being found at node $|j\rangle$ at time t can thus be given by $|\langle j|e^{-iHt}|\psi(0)\rangle|^2$.

Now, let the quantum walker be initialized in momentum eigenstate $|k\rangle$ incident from the left; this results in a time-independent scattered state of the form

$$|\psi_s\rangle = \hat{U}|k\rangle = \begin{cases} |k\rangle + r(k)|-k\rangle, & j \leqslant d \\ t(k)|k\rangle, & j > d \end{cases} \tag{6}$$

(the *Bethe ansatz*), where $t(k)|k\rangle$ and $r(k)|-k\rangle$ are the transmitted and reflected components, respectively. It was shown by Childs *et al.* [3] in the context of algorithmic speedup that, given $|\psi_s(k)\rangle$ remains an eigenstate of $H = H_0 + \Gamma$, a pair of linearly independent equations are produced which uniquely determine $t(k)$ and $r(k)$. This was further extended by Farhi *et al.* [10] in order to calculate the transmission probability due to finite trees and semi-infinite lines attached at singular nodes. Finally, it was demonstrated by Li *et al.* [37] that, in the presence of double diagonal defects, a CTQW system exhibits resonance behavior determined inherently by the nature of the discrete space. In successive sections, we will determine analytic expressions for the complete set of eigenstates for a single defect and relate this to group velocity. Moreover, we will show through analytical derivations that this previously established resonant behavior exists in the case of multiple sets of defects, and describe an efficient numerical method for exploring systems with arbitrary distributions of diagonal defects.

III. SINGLE-DEFECT EIGENSTATES

Using the diagonal defect model defined above for a CTQW containing a single-point defect on an infinite line, the Hamiltonian can therefore be written as

$$H = \sum_j (2|j\rangle\langle j| - |j-1\rangle\langle j| - |j+1\rangle\langle j|) + \alpha|d\rangle\langle d|. \tag{7}$$

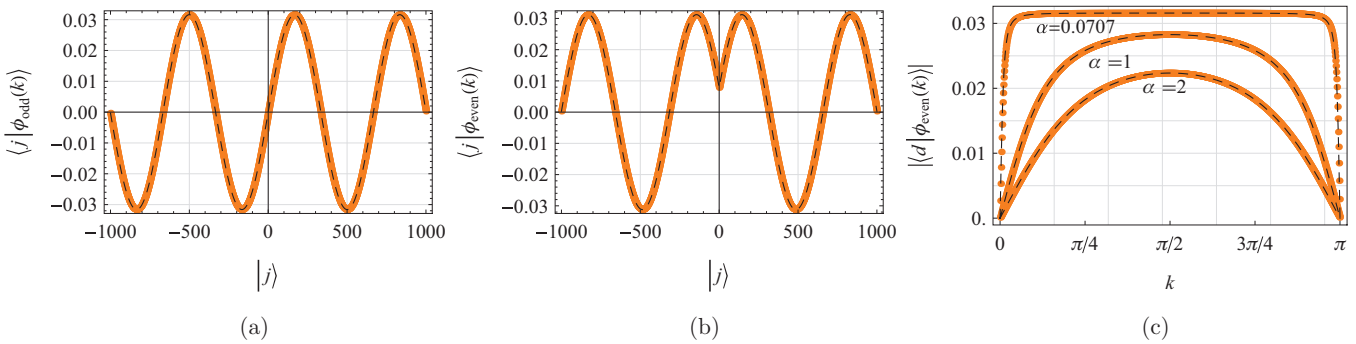

FIG. 1. (Color online) The numeric (orange solid line) and analytic (black dashed line) single-point-defect eigenstates are plotted for the set of (a) odd continuous eigenstates and (b) even continuous eigenstates. (c) The value of the even states at the defect location $|0\rangle$ for defect strength $\alpha = 1/\sqrt{200}, 1, 2$.

For simplicity, and without loss of generality, choose $d = 0$. Now let $|\phi\rangle$ denote the eigenstates of the Hamiltonian, with associated eigenvalues $\lambda \in \mathbb{R}$; i.e., $H|\phi\rangle = \lambda|\phi\rangle$. Expanding $\langle j|H|\phi\rangle$ explicitly using Eq. (7) and the position state decomposition of the eigenstates, $|\phi\rangle = \sum_{j'} |j'\rangle\langle j'|\phi\rangle = \sum_{j'} c_{j'}|j'\rangle$, we arrive at the following recurrence relation:

$$\begin{aligned}\langle j|H|\phi\rangle &= 2c_j - c_{j-1} - c_{j+1} + \alpha c_0 \delta_{j0} \\ &= \lambda c_j \Rightarrow (2-\lambda)c_j - c_{j-1} - c_{j+1} = \alpha c_0 \delta_{j0}. \end{aligned} \quad (8)$$

We now have an inhomogeneous, linear recurrence equation with constant coefficients—this equation fully determines the eigenstates and eigenvalues of the system. By substituting in the ansatz $c_j = r^j$ [20], we readily see that the general *homogeneous* solution is

$$\begin{aligned} c_j &= A r_-^j + B r_+^j \\ &= 2^{-j} A (2 - \lambda - \sqrt{\lambda - 4}\sqrt{\lambda})^j \\ &\quad + 2^{-j} B (2 - \lambda + \sqrt{\lambda - 4}\sqrt{\lambda})^j, \end{aligned} \quad (9)$$

where A and B are as yet undetermined functions of α and λ. Using this result as a basis to calculate inhomogeneous solutions to Eq. (8), we must consider regimes where both oscillatory and bound solutions exist.

A. Continuous eigenstates

To determine the continuous eigenstates, consider oscillating solutions of Eq. (9). It is clear that a necessary requirement for oscillating solutions is $|r_\pm| \leqslant 1$; this is satisfied only for $0 \leqslant \lambda \leqslant 4$. For convenience, the parametrization $\lambda = 2(1 - \cos k)$, $0 \leqslant k \leqslant \pi$, can be used, resulting in a homogeneous solution of the form

$$c_j = A e^{-ikj} + B e^{ikj}. \quad (10)$$

The method of undetermined coefficients can now be used to calculate the inhomogeneous solutions to the system in this λ regime. We find that two solutions exist, with odd and even symmetry around the defect, respectively:

$$\begin{aligned} \langle j|\phi_{\rm odd}(k)\rangle &= \frac{1}{\sqrt{\pi}} \sin kj, \quad 0 \leqslant k \leqslant \pi, \\ \langle j|\phi_{\rm even}(k)\rangle &= \frac{1}{\sqrt{\pi}} t_\alpha(k) \left(\frac{1}{2} \alpha \csc k \sin k|j| + \cos kj \right), \\ &\quad 0 \leqslant k \leqslant \pi, \end{aligned} \quad (11)$$

where $t_\alpha(k) = 1/[1 + \frac{1}{2} i\alpha \csc k]$ is simply the transmission coefficient of the CTQW incident on a single defect. Also recall that, by construction, both eigenstates satisfy the eigenvalue equation

$$H|\phi(k)\rangle = \lambda(k)|k\rangle, \quad \lambda(k) = 2(1 - \cos k)|k\rangle \quad (12)$$

(as is expected, the eigenvalues are of the same form as Koster and Slater [20] and Merrifield [21] in the case where the lattice parameter $\alpha \to 1$). Comparing these results to those obtained by numerical analysis (Fig. 1) verifies that these eigenstates do, in fact, represent the complete set of continuous eigenstates. Furthermore, it can be seen that setting $\alpha = 0$ does, indeed, recover the free-space eigenstates $|k\rangle$, $k \in [-\pi, \pi]$.

B. Bound states

For bound-state $|\phi_B\rangle$ solutions to Eq. (8) to be physical, it is required that $\langle j|\phi_B\rangle \to 0$ as $j \to \pm\infty$. Restricting our attention to $\lambda < 0$, $\lambda > 4$, the method of undetermined coefficients is applied in the case of odd symmetry and even symmetry ($j \to |j|$). As in the continuous case, both odd and even bound states exist, with respective conditions $A + B = 0$ and $A = B(\sqrt{\lambda - 4}\sqrt{\lambda} - \alpha)/(\sqrt{\lambda - 4}\sqrt{\lambda} + \alpha)$.

By taking into account the boundary condition, the odd bound state turns out to be nonphysical [$r_-(j) - r_+(j)$ diverges as $j \to \pm\infty$] and must be discarded. The even bound state, of the form

$$\begin{aligned} \langle j|\phi_B\rangle &= A r_-(|j|) + B r_+(|j|) \\ &= B r_-(|j|) \frac{\sqrt{\lambda - 4}\sqrt{\lambda} - \alpha}{\sqrt{\lambda - 4}\sqrt{\lambda} + \alpha} + B r_+(|j|), \end{aligned} \quad (13)$$

contains only one divergent term [$r_-(|j|)$] and thus represents a physical bound state when the coefficient of $r_-(|j|)$ is zero for all values of α; thus, $\lambda = 2 + \alpha\sqrt{1 + 4/\alpha^2}$. Substituting this back into Eq. (13) and normalizing, the bound state of the system is therefore given by

$$\langle j|\phi_B\rangle = \frac{2^{-|j|}\sqrt{|\alpha|}}{(\alpha^2 + 4)^{1/4}} \left(\alpha - \alpha\sqrt{1 + \frac{4}{\alpha^2}} \right)^{|j|}, \quad (14)$$

satisfying the eigenvalue equation

$$H|\phi_B\rangle = \lambda_\alpha |\phi_B\rangle, \quad \lambda_\alpha = 2 + \alpha\sqrt{1 + \frac{4}{\alpha^2}}. \quad (15)$$

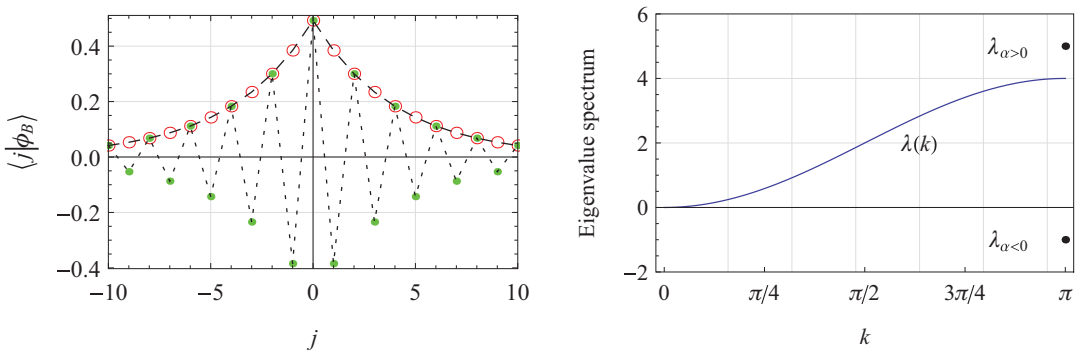

FIG. 2. (Color online) Left: The numeric and analytic single-point defect bound states are plotted and compared for the cases (i) $\alpha < 0$ with the analytic result in long-dashed black lines and the numerical data points in red open circles, and (ii) $\alpha > 0$ with the analytic result in short-dashed black lines and the numerical data points in green dots. Right: The complete eigenvalue spectrum of the Hamiltonian with a single-point defect.

Some properties of the single-defect bound state that can be ascertained from the analytic expression include (1) in the limit $|\alpha| \to \infty$, $\langle j-d|\phi_B\rangle \to \delta_{jd}$ and $\lambda_\alpha \to \infty$ (i.e., the contribution of the bound state to the time evolution of a CTQW outweighs that of the continuous eigenstates for large α) and (2) in the limit $\alpha \to 0$, $\langle j-d|\phi_B\rangle \to 0$ and $\lim_{\alpha\to 0^-}\lambda_\alpha = 0$, $\lim_{\alpha\to 0^+}\lambda_\alpha = 4$ (i.e., the contribution of the bound state to the time evolution of a CTQW is approximately the trivial solution for small α and can be neglected). It should also be noted that for $\alpha > 0$, the bound-state amplitude shows damped oscillating behavior; this is not the case for $\alpha < 0$ (Fig. 2). However, in both cases, the probability distributions $|\langle v_j|\phi_B\rangle|^2$ are equal.

C. Eigenstate completeness and time evolution

Using the orthogonality relations of the sine and cosine functions, it can be shown that the eigenstates calculated above remain orthonormal with respect to each other; that is, for all values of $0 \leqslant k \leqslant \pi$ and $\alpha \in \mathbb{R}$, $\langle\phi_{\text{odd}}(k)|\phi_B\rangle = 0, \langle\phi_{\text{even}}(k)|\phi_B\rangle = 0,$ and $\langle\phi_{\text{odd}}(k)|\phi_{\text{even}}(k)\rangle = 0$. Coupling these results with the completeness of Hermitian eigenstates, the identity operator for the single defect containing discrete space can be written as

$$\hat{I} = \int_0^\pi dk\,(|\phi_{\text{odd}}(k)\rangle\langle\phi_{\text{odd}}(k)| + |\phi_{\text{even}}(k)\rangle\langle\phi_{\text{even}}(k)|) + |\phi_B\rangle\langle\phi_B|, \tag{16}$$

and thus the time-evolution operator $\hat{U}(t) \equiv e^{-iHt} = e^{-iHt}\hat{I}$ has the form

$$\hat{U}(t) = \int_0^\pi dk e^{-2it(1-\cos k)}[|\phi_{\text{odd}}(k)\rangle\langle\phi_{\text{odd}}(k)| + |\phi_{\text{even}}(k)\rangle\langle\phi_{\text{even}}(k)|] + e^{-i\lambda_\alpha t'}|\phi_B\rangle\langle\phi_B|. \tag{17}$$

This integral form of the time-evolution operator now enables us to construct an expression for the time evolution of an arbitrary state $|\psi\rangle$ from time t to t',

$$\langle j'|e^{-iHt'}|\psi(t)\rangle = \sum_j \int_0^\pi dk G_{\alpha,d}(j',t';j;k)\langle j|\psi(t)\rangle, \tag{18}$$

where

$$G_{\alpha,d}(j',t';j;k) = \frac{1}{\pi}e^{-2it'(1-\cos k)}\Big[\sin k(j'-d)\sin k(j-d) + \frac{1}{4}|t_\alpha(k)|^2\epsilon(j'-d)\epsilon(j-d)\Big] + e^{-i\lambda_\alpha t}\delta(k-1)\phi_B(j-d)\phi_B(j'-d), \tag{19}$$

with $t_\alpha(k) = 1/[1+(i\alpha/2)\csc k]$, $\epsilon(j) = \alpha\csc k\sin k|j| + 2\cos kj$, $\lambda_\alpha = 2+\alpha\sqrt{1+4/\alpha^2}$, $\phi_B(j) = \frac{2^{-|j|}\sqrt{|\alpha|}}{(\alpha^2+4)^{1/4}}(\alpha - \alpha\sqrt{1+4/\alpha^2})^{|j|}$, $|d\rangle$ the location of the defect, and α the defect amplitude.

Using this integral approach, $\langle j'|e^{-iHt'}|\psi\rangle$ is plotted in the case of $\alpha = 1/\sqrt{2}$, $d = 5$, $|\psi\rangle = |v_1\rangle$, and $t' = 20$ in Fig. 3. It can be seen that the integral and the matrix exponential method are in excellent agreement.

The Green's function offers other advantages compared to the previously considered one. For instance, it is now well defined in the case of the initial state being at the vertex containing the defect, and the form of the expression is the same over all space (i.e., there are no piecewise components and no need to separate the position space into a "transmitted region," "reflected region," etc.). Numerous advantages also exist compared to the matrix exponential method: the time evolution can now be explored on a vertex by vertex basis (reducing computation time as we no longer need to consider the entire discrete subspace), numerical integration is less computationally expensive and easier to implement, and asymptotic approximations of the integral can be used to characterize behavior for large or small t and α, among others.

IV. MULTIPLE DEFECTS

Using the same mathematical scaffolding discussed in Sec. II and extending the work of Li *et al.* [37] to multiple defects, the transmission coefficient for N point defects, located at vertices $d_0, \ldots, d_i, \ldots, d_{N-1}$, can be calculated by

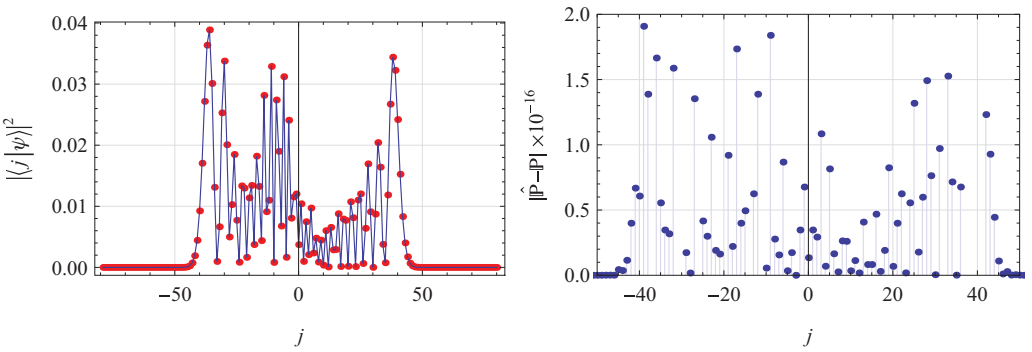

FIG. 3. (Color online) (a) The time evolution of the initial state $|1\rangle$ for time $t' = 20$, with a defect placed at $d = 5$ with strength $\alpha = 1/\sqrt{2}$, using the matrix exponential definition (blue line) and the integral approach (18) (red data points). (b) A plot of the absolute error between both methods.

starting with the scattered state ansatz,

$$|\psi_s(k)\rangle = \begin{cases} |k\rangle + r_1(k)|-k\rangle, & j < d_0 \\ \vdots & \\ t_i(k)|k\rangle + r_{i+1}|-k\rangle, & d_{i-1} < j < d_i \\ \vdots & \\ t_N(k)|k\rangle, & d_{N-1} \leqslant j. \end{cases} \tag{20}$$

The Hamiltonian of the system is now given by

$$H = \sum_j (2|j\rangle\langle j| - |j-1\rangle\langle j| - |j+1\rangle\langle j|) + \sum_{i=0}^{N-1} \alpha_i |d_i\rangle\langle d_i|, \tag{21}$$

and so the eigenvalue condition,

$$\frac{\langle j|H|\psi_s(k)\rangle}{\langle j|\psi_s(k)\rangle} = 2(1-\cos k)$$

(which must hold for all $j \in \mathbb{Z}$ and $-\pi \leqslant k < \pi$), can then be applied to all possible regions described by Eq. (20). As before, this produces a set of $2N$ linearly independent linear equations relating $t_1(k), \ldots, t_N(k), r_1(k), \ldots, r_N(k)$, which can then be solved to calculate all the transmission and reflection amplitudes. Note that there is the added caveat that as N increases, the complexity of the analytic form of $t_i(k)$ and $r_i(k)$ appears to drastically increase—suggesting that for N significantly large, analytic approximations or numerical methods may be preferable.

Using this method, the transmission coefficient was calculated in the case of the 2, 3, 5, and 8-point defects, respectively. For convenience, allowing $d_{i+1} - d_i = L$ and $\alpha_i = \alpha \forall i$ (i.e., all barriers have equal separation and amplitude), the transmission amplitude is given by

$$t_N(k) = \frac{1}{1+\omega_N} \Rightarrow T_N(k) = |t_N(k)|^2 = \frac{1}{1+\Omega_N}, \tag{22}$$

where

$$\omega_2 = i\alpha \csc k + \tfrac{1}{4}\alpha^2(e^{2ikL} - 1)\csc^2 k, \tag{23a}$$

$$\begin{aligned}\omega_3 = -\tfrac{1}{8} i\alpha e^{2ikL} \csc^3 k [&2\cos 2kL(\alpha^2 - 2i\alpha \sin k - 3) \\ &+ 4\alpha \sin k(i - 2\sin 2kL) - 3i \sin 2k(L+1) \\ &+ 6i \sin 2kL - 3i \sin 2k(L-1) + 3\cos 2k(L-1) \\ &+ 3\cos 2k(L+1) - 2\alpha^2],\end{aligned} \tag{23b}$$

and thus

$$\Omega_2 = \tfrac{1}{4}\alpha^2 \csc^4 k(\alpha \sin kL + 2\sin k \cos kL)^2, \tag{24a}$$

$$\begin{aligned}\Omega_3 = \tfrac{1}{16}\alpha^2 \csc^6 k[&(\alpha^2 - 2)\cos 2kL - 4\alpha \sin k \sin 2kL \\ &+ \cos 2k(L-1) + \cos 2k(L+1) + \cos 2k - \alpha^2 - 1]^2.\end{aligned} \tag{24b}$$

The analytic form of $T(k)$ for the 5- and 8-point defect is too long and complex to be reproduced here. The transmission coefficients for $N = 2,3,5$, and 8 are plotted and compared in Fig. 4 for barrier strength $\alpha = 1$ and separations of $L = 0,1,2$, and 5. It can be seen that as $N \to \infty$, the local minimums of $T(k)$ approach zero, while the resonant peaks widen. Furthermore, oscillation amplitudes appear to decrease, and the transition between regions of perfect and zero transmission becomes much sharper. Qualitatively, this appears indicative of the electronic band structure observed in continuous-space models of crystal lattices. The results are also visualized in Fig. 5, showing the effect of defect amplitude α on the transmission coefficient for the case $N = 8$. It is easily seen that, by altering α, a method is provided to control the placement and size of the unity transmission band.

Ultimately, however, this method of calculating the transmission for N defects becomes unwieldy for large N, as the increasing number of linearly independent equations required to calculate $r_i(k), t_i(k)$ scales by $O(2N)$ and results in drastically larger computation times. Further, we are usually only interested in calculating $r_1(k)$ and $t_N(k)$; this motivates the creation of an algorithm to more efficiently characterize CTQW transmission through multiple arbitrary defects.

V. A GENERAL NUMERICAL APPROACH FOR MULTIPLE DEFECTS

In the case of continuous-space quantum mechanics, the Fourier method approach utilized by Yiu and Wang [38],

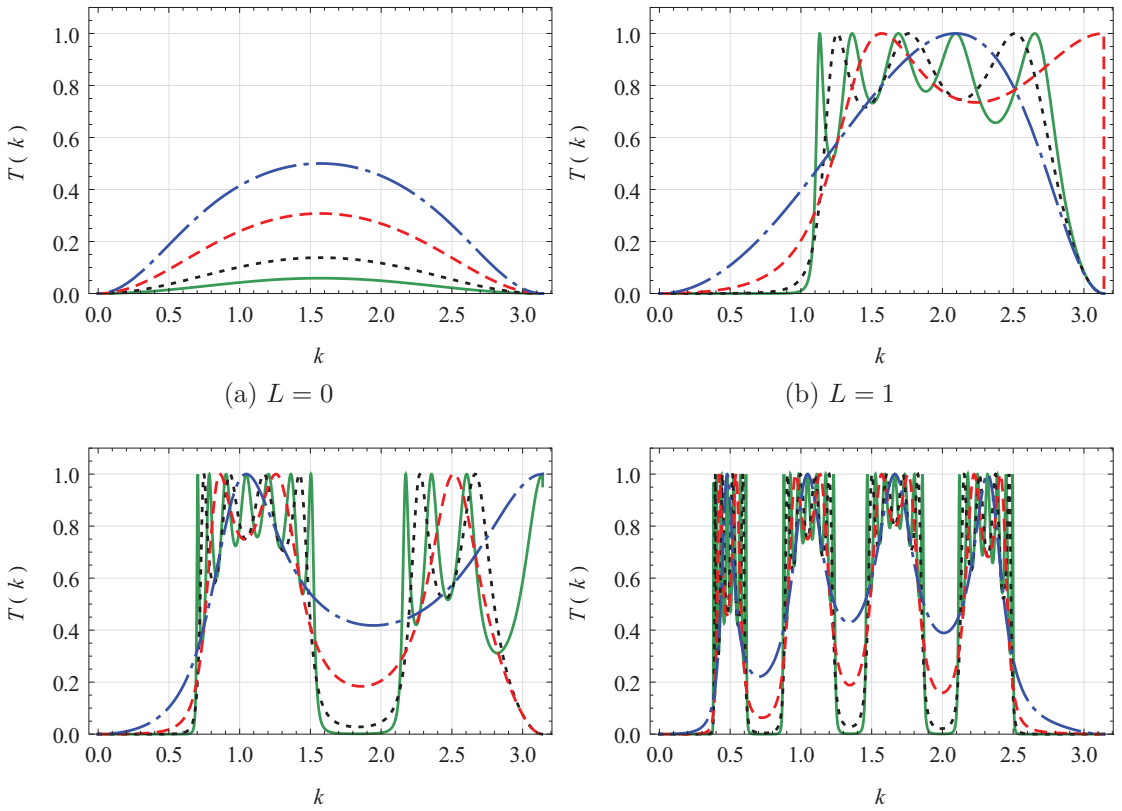

(a) $L = 0$ (b) $L = 1$

(c) $L = 2$ (d) $L = 5$

FIG. 4. (Color online) Transmission coefficient vs momentum for a CTQW momentum eigenstate incident on an N-point defect, where $N = 2$ (blue dot-dashed line), $N = 3$ (red dashed line), $N = 5$ (black dotted line), and $N = 8$ (green solid line). The defect-induced barriers are constructed with unity amplitude ($\alpha = 1$) and equal separation L.

Falloon and Wang [39], and Manouchehri and Wang [40] provides an efficient method of numerically calculating the transmission coefficient $T(k)$ over a wide range of k. In this section, this method will be adapted for the CTQW on the infinite line and verified against the multibarrier analytic solution derived in the previous section.

Consider an arbitrary initial state $|\psi_0\rangle$ incident on a set of defects or barriers, with the transmitted component denoted $|\psi_t\rangle$ and produced as per the transmission amplitude $t(k)$. Using the completeness of the momentum eigenstates, these can be written as

$$|\psi_0\rangle = \frac{1}{2\pi}\int_{-\pi}^{\pi} dk|k\rangle\langle k|\psi_0\rangle, \quad |\psi_t\rangle = \frac{1}{2\pi}\int_{-\pi}^{\pi} dk|k\rangle\langle k|\psi_t\rangle. \tag{25a}$$

Evolving the state $|\psi_0\rangle$ through time via the unitary operator $\hat{U}_t$, which acts to separate out the transmitted component,

$$|\psi_t\rangle = \hat{U}_t|\psi_0\rangle = \frac{1}{2\pi}\int_{-\pi}^{\pi} dk\hat{U}_t|k\rangle\langle k|\psi_0\rangle$$
$$= \frac{1}{2\pi}\int_{-\pi}^{\pi} dkt(k)|k\rangle\langle k|\psi_0\rangle, \tag{26}$$

and comparing this with Eq. (25a), it can be seen that we require

$$\langle k|\psi_t\rangle = t(k)\langle k|\psi_0\rangle \Rightarrow T(k) = |t(k)|^2 = \frac{|\langle k|\psi_t\rangle|^2}{|\langle k|\psi_0\rangle|^2}. \tag{27}$$

Using position space completeness ($\hat{I} = \sum_j |v_j\rangle\langle v_j|$) coupled with the inner product $\langle k|v_j\rangle = e^{-ikj}$, this expression can be evaluated explicitly in terms of probability amplitudes of the walker at each vertex:

$$T(k) = \frac{|\langle k|\psi_t\rangle|^2}{|\langle k|\psi_0\rangle|^2} = \frac{\left|\sum_j e^{-ikj}\langle j|\psi_t\rangle\right|^2}{\left|\sum_j e^{-ikj}\langle j|\psi_0\rangle\right|^2}. \tag{28}$$

The numerical calculation of the inner product $\langle j|\psi_t\rangle = \langle j|e^{-iHt}|\psi_0\rangle$ is performed by expanding the matrix exponential via the Chebyshev expansion scheme, as detailed in Wang and Scholz [41]. This method is particularly beneficial for two major reasons: first, since the coefficients of the expansion are Bessel functions, they vanish after a finite number of terms, allowing for an exceptionally high level of accuracy with a comparatively small number of terms. Second, this is an example of a global propagator, negating the need for iterative calculations at smaller time steps which can introduce accumulation error.

Briefly outlining the expansion, we have

$$U_t \equiv e^{-iHt/\hbar}$$
$$= e^{-i(\lambda_{\max}+\lambda_{\min})t/2}\left[J_0(\eta)\phi_0(-i\tilde{H}) + 2\sum_{n=1}^{\infty} J_n(\eta)\phi_n(-i\tilde{H})\right], \tag{29}$$

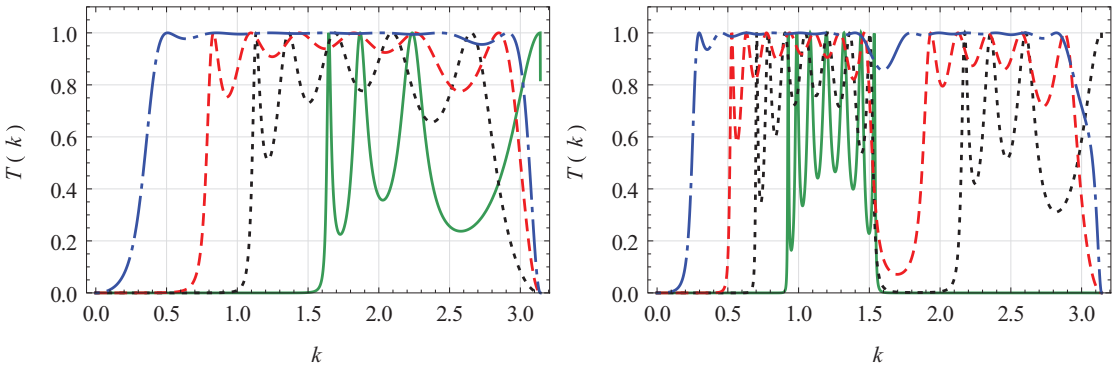

(a) $L = 1$ (b) $L = 2$

FIG. 5. (Color online) Transmission coefficient vs momentum for a CTQW momentum eigenstate incident on an evenly spaced 8-point defect, with barrier amplitudes $\alpha = 0.1$ (blue dot-dashed line), $\alpha = 0.5$ (red dashed line), $\alpha = 1$ (black dotted line), and $\alpha = 2$ (green solid line).

where $\lambda_{\max}$ and $\lambda_{\min}$ are maximum and minimum eigenvalues of the Hamiltonian matrix H, $\eta = (\lambda_{\max} - \lambda_{\min})t/2$, $J_n(\eta)$ are the Bessel functions of the first kind, and ϕ_n are the Chebyshev polynomials. To ensure convergence, the Hamiltonian needs to be normalized as

$$\widetilde{\mathcal{H}} = \frac{1}{\lambda_{\max} - \lambda_{\min}}[2H - \lambda_{\max} - \lambda_{\min}]. \tag{30}$$

This method can now be used to investigate the behavior of a CTQW on an infinite line, incident on an arbitrary distribution of diagonal defects. However, for comparison purposes, we will restrict our attention to N equally spaced diagonal defects. The Hamiltonian under investigation is therefore given by

$$H = \sum_j (2|j\rangle - |j-1\rangle - |j+1\rangle)\langle j| + \sum_{n=0}^{N-1} \alpha_n |d+nL\rangle\langle d+nL|, \tag{31}$$

where $\alpha_n \in \mathbb{R}$ represents the amplitude of the nth defect, $d \in \mathbb{Z}$ is the position of the first defect, and $L \in \mathbb{N}$ is the integer spacing between defects. For convenience, the initial state is chosen such that the walker is localized at a vertex to the left of the double reflecting barriers, i.e., $|\psi(0)\rangle = |v_{j'}\rangle$, $j' < 0$.

Noting that

$$\left|\sum_j e^{-ikj}\langle j|j'\rangle\right|^2 = \left|\sum_j e^{-ikj}\delta_{jj'}\right|^2 = |e^{-ikj'}|^2 = 1 \forall k \in [-\pi,\pi), \tag{32}$$

this allows the expression for the transmission coefficient give by Eq. (28) to reduce to

$$T(k) = \left|\sum_j e^{-ikj}\langle j|\psi_t\rangle\right|^2 \quad \forall k \in [-\pi,\pi). \tag{33}$$

Using Eq. (29), $T(k) = |\sum_j e^{-ikj}\langle j|e^{-iHt}|j'\rangle|^2$ is calculated for $t = 300$, chosen sufficiently large such that the probability of the walker remaining located between the defects is small, i.e., $\sum_{j=0}^{(N-1)L} |\langle d+j|\psi(t)\rangle|^2 \approx 0$. The results are plotted in Fig. 6 for a variety of different values of L and compared to the analytic solution derived in Sec. IV. It is observed that the numeric results closely match the analytic solutions, with an average absolute difference of $\sigma_T = 2.64 \times 10^{-3}$. As an aside, note the presence of Gibbs phenomenon at the boundaries of the domain due to the use of Fourier methods. By restricting the analysis to $0.5 < k < 2.5$, the absolute difference between the numeric and analytic

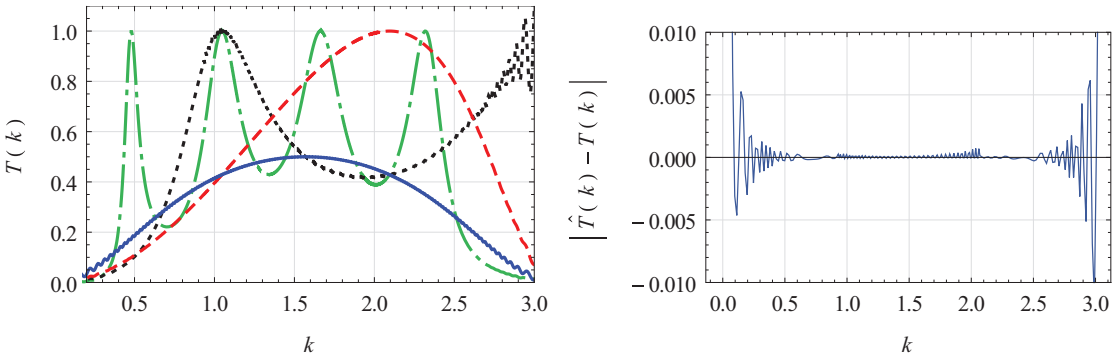

FIG. 6. (Color online) (a) Transmission coefficient vs momentum of a CTQW momentum eigenstate incident on two defects of unity amplitude, separated by distances $L = 0$ (solid blue line), $L = 1$ (dashed red line), $L = 2$ (dotted black line), and $L = 5$ (dot-dashed green line), and calculated via numerical Fourier methods. (b) Absolute difference between numeric and analytic results for the case $L = 1$.

results reduces to $\sigma_T = 3.58 \times 10^{-7}$. This general numerical approach can now be applied to situations where analytical analysis becomes impossible, fine tuning the parameters to increase accuracy.

It should be noted that a major source of error associated with this method is due to a nonzero probability distribution located between defects at measurement time. While this can be avoided by increasing the time step t, it requires that a larger number of vertices be included in the propagation grid, as well as an increase in the number of Chebyshev summation terms required for significant accuracy, potentially increasing the computational time. The additional computational time may prove insignificant with the accelerating availability of computational power. If not, further refinements (such as absorbing boundary conditions and multiple passes) may be needed.

VI. CONCLUSIONS

In the past two decades, quantum walks have played a pivotal role in the field of quantum information theory and current research is suggesting potential applications across a whole range of different fields, making them an invaluable tool in the study of structured, discrete-space systems. Significant advances are also constantly being made in experimental realizations of quantum walks, providing a means to fully utilize the computational power of quantum walkers, while simultaneously requiring an accurate theoretical and efficient numerical framework to provide detailed information on the effects of disorder and scattering on a quantum walk.

In this paper, a one-dimensional continuous-time quantum walk in the presence of multiple defects was explored analytically, with the results highlighting resonance behavior previously observed in the case of double diagonal defects. It was also demonstrated that by increasing the number of defects and by altering the defect amplitudes, "bands" of perfect transmission (surrounded by regions of zero transmission) can be selectively placed in momentum space, allowing for a high level of control of quantum walking characteristics. This provides a link between the tight-binding lattice models widely used in condensed matter physics and the development of quantum information applications based on continuous-time quantum walks. Finally, we extended the Fourier-Chebychev method utilized in the literature for continuous position space to the discrete space of CTQWs, which provides a general numerical approach to situations where analytical analysis becomes impossible, such as multiple barriers, higher dimensions, and multiple interacting walkers.

Quantum walks remain an important field of study due to their crucial role in both quantum information processing and the modeling of complex quantum systems. As a result of this research, we hope to provide methods to selectively control and efficiently characterize the time evolution of quantum walks by taking advantage of diagonal disorder that can sometimes be unavoidable in physical systems.

ACKNOWLEDGMENT

J.A.I. would like to thank the Hackett Foundation and the University of Western Australia for financial support.

[1] Y. Aharonov, L. Davidovich, and N. Zagury, Phys. Rev. A **48**, 1687 (1993).
[2] J. Kempe, Contemp. Phys. **44**, 307 (2003).
[3] A. M. Childs, R. Cleve, E. Deotto, E. Farhi, S. Gutmann, and D. A. Spielman, *Proceedings of the Thirty-Fifth Annual ACM Symposium on Theory of Computing STOC '03* (ACM, New York, 2003), pp. 59–68.
[4] A. M. Childs and J. Goldstone, Phys. Rev. A **70**, 022314 (2004).
[5] S. D. Berry and J. B. Wang, Phys. Rev. A **83**, 042317 (2011).
[6] S. D. Berry and J. B. Wang, Phys. Rev. A **82**, 042333 (2010).
[7] J. K. Gamble, M. Friesen, D. Zhou, R. Joynt, and S. N. Coppersmith, Phys. Rev. A **81**, 052313 (2010).
[8] B. L. Douglas and J. B. Wang, J. Phys. A: Math. Theor. **41**, 075303 (2008).
[9] A. M. Childs, Phys. Rev. Lett. **102**, 180501 (2009).
[10] E. Farhi, J. Goldstone, and S. Gutmann, arXiv:quant-ph/0702144.
[11] A. M. Childs and D. Gosset, J. Math. Phys. **53**, 102207 (2012).
[12] F. W. Strauch, Phys. Rev. A **74**, 030301(R) (2006).
[13] Y. Bromberg, Y. Lahini, R. Morandotti, and Y. Silberberg, Phys. Rev. Lett. **102**, 253904 (2009).
[14] A. Peruzzo, M. Lobino, J. C. F. Matthews, N. Matsuda, A. Politi, K. Poulios, X. Zhou, Y. Lahini, N. Ismail, K. Wörhoff, Y. Bromberg, Y. Silberberg, M. G. Thompson, and J. L. O'Brien, Science **329**, 1500 (2010).
[15] L. Sansoni, F. Sciarrino, G. Vallone, P. Mataloni, A. Crespi, R. Ramponi, and R. Osellame, Phys. Rev. Lett. **108**, 010502 (2012).
[16] J. D. A. Meinecke, K. Poulios, A. Politi, J. C. F. Matthews, A. Peruzzo, N. Ismail, K. Wörhoff, J. L. O'Brien, and M. G. Thompson, Phys. Rev. A **88**, 012308 (2013).
[17] M. A. Broome, A. Fedrizzi, B. P. Lanyon, I. Kassal, A. Aspuru-Guzik, and A. G. White, Phys. Rev. Lett. **104**, 153602 (2010).
[18] M. Karski, L. Förster, J. Choi, A. Steffen, W. Alt, D. Meschede, and A. Widera, Science **325**, 174 (2009).
[19] H. Schmitz, R. Matjeschk, C. Schneider, J. Glueckert, M. Enderlein, T. Huber, and T. Schaetz, Phys. Rev. Lett. **103**, 090504 (2009).
[20] G. F. Koster and J. C. Slater, Phys. Rev. **95**, 1167 (1954).
[21] R. E. Merrifield, J. Chem. Phys. **38**, 920 (1963).
[22] P. Dean, Proc. Phys. Soc. **73**, 413 (1959).
[23] D. J. Thouless, J. Phys. C **5**, 77 (1972).
[24] I. Avgin and D. Huber, J. Lumin. **129**, 1916 (2009).
[25] Y. Yin, D. E. Katsanos, and S. N. Evangelou, Phys. Rev. A **77**, 022302 (2008).
[26] A. Schreiber, K. N. Cassemiro, V. Potoček, A. Gábris, I. Jex, and C. Silberhorn, Phys. Rev. Lett. **106**, 180403 (2011).
[27] O. Mülken and A. Blumen, Phys. Rep. **502**, 37 (2011).
[28] J. P. Keating, N. Linden, J. C. F. Matthews, and A. Winter, Phys. Rev. A **76**, 012315 (2007).
[29] E. Farhi and S. Gutmann, Phys. Rev. A **58**, 915 (1998).

[30] E. Agliari, A. Blumen, and O. Mülken, Phys. Rev. A **82**, 012305 (2010).
[31] G. S. Engel, T. R. Calhoun, E. L. Read, T. Ahn, T. Mančal, Y. Cheng, R. E. Blankenship, and G. R. Fleming, Nature (London) **446**, 782 (2007).
[32] E. Collini, C. Y. Wong, K. E. Wilk, P. M. G. Curmi, P. Brumer, and G. D. Scholes, Nature (London) **463**, 644 (2010).
[33] D. Mi, G. Liu, J. Wang, and Z. Li, J. Theor. Biol. **241**, 152 (2006).
[34] D. Mi, W. Q. Meng, and Y. Q. Sun, Phys. Rev. E **83**, 041901 (2011).
[35] O. Mülken, A. Blumen, T. Amthor, C. Giese, M. Reetz-Lamour, and M. Weidemüller, Phys. Rev. Lett. **99**, 090601 (2007).
[36] A. M. Childs, D. Gosset, and Z. Webb, Science **339**, 791 (2013).
[37] Z. J. Li, J. A. Izaac, and J. B. Wang, Phys. Rev. A **87**, 012314 (2013).
[38] C. Yiu and J. Wang, J. Appl. Phys. **80**, 4208 (1996).
[39] P. E. Falloon and J. B. Wang, Comput. Phys. Commun. **134**, 167 (2001).
[40] K. Manouchehri and J. B. Wang, J. Comput. Theor. Nanosci. **3**, 249 (2006).
[41] J. B. Wang and T. T. Scholz, Phys. Rev. A **57**, 3554 (1998).